BNL-41894

NUCLEAR PHYSICS WITH STRANGE PARTICLES

Carl B. Dover

Physics Department
Brookhaven National Laboratory
Upton, New York 11973

BNL--41894

DE89 002912

ABSTRACT

Recent progress in the understanding of strange particle interactions with nuclear systems is reviewed. We discuss the relative merits of various reactions such as $(K^-, \pi^\pm)$, (π^+, K^+) or (γ, K^+) for hypernuclear production. The structure of ${}^{13}_{\Lambda}C$ is analyzed in some detail, in order to illustrate the role of the ΛN residual interaction and approximate dynamical symmetries in hypernuclear structure. Recent results on the single particle states of a Λ in heavy systems, as revealed by (π^+, K^+) reaction studies, are used to extract information on the density dependence and effective mass which characterize the Λ-nucleus mean field. Finally, we develop the idea that K^+-nucleus scattering at low energies is sensitive to the subtle "swelling" effects for nucleons bound in nuclei.

Lectures given at the International School of
Intermediate Energy Nuclear Physics
Venice, Italy
July 6 – 16, 1988

This work has been supported by the U. S. Department of Energy under contract no. DE-AC02-76CH00016.

NUCLEAR PHYSICS WITH STRANGE PARTICLES

Carl B. Dover
Physics Department
Brookhaven National Laboratory
Upton, New York 11973

ABSTRACT

Recent progress in the understanding of strange particle interactions with nuclear systems is reviewed. We discuss the relative merits of various reactions such as $(K^-, \pi^\pm)$, (π^+, K^+) or (γ, K^+) for hypernuclear production. The structure of ${}^{13}_{\Lambda}C$ is analyzed in some detail, in order to illustrate the role of the ΛN residual interaction and approximate dynamical symmetries in hypernuclear structure. Recent results on the single particle states of a Λ in heavy systems, as revealed by (π^+, K^+) reaction studies, are used to extract information on the density dependence and effective mass which characterize the Λ–nucleus mean field. Finally, we develop the idea that K^+–nucleus scattering at low energies is sensitive to the subtle "swelling" effects for nucleons bound in nuclei.

1. INTRODUCTION AND MOTIVATION

The focus of these lectures is on the interactions of strange particles with nuclear systems. These include both kaons $(K^\pm)$ and hyperons (Λ, Σ, Ξ). The kaons are members of the $J^\pi = 0^-$ pseudoscalar meson nonet of SU(3), along with $\{\pi, \eta, \eta'\}$, while the Λ, Σ and Ξ are classified in the $J^\pi = \frac{1}{2}^+$ baryon octet with the nucleon (N). The quark flavor content is as follows: $K^- = s\bar{u}$, $\Lambda = s\,(ud)_{I=0}$, $\Sigma = s\,(ud)_{I=1}$, *etc.*, where "s" stands for a strange quark. Thus, the spectroscopy of a Λ or Σ embedded in a nucleus is sometimes referred to as that of a "tagged strange quark." The study of the response of a many–body system to a hyperon "impurity" sheds light on the role of strange quarks in strong interactions, *i.e.* the SU(3) structure of baryon–baryon interactions, and, in principle, on properties of the nucleus itself, such as compressibility, moment of inertia, *etc.* At the hadron level, the Λ is distinguishable from the nucleon, so it is allowed to occupy any single particle orbital in the nucleus, without the constraints of the Pauli principle. This single particle structure is in fact observed: even in the $1s$ orbit in heavy nuclei, the Λ retains its distinguishable character, thus providing one of the best examples of single particle shell structure in nuclear physics. At the quark level, one might

This work has been supported by the U. S. Department of Energy under contract no. DE-AC02-76CH00016.

anticipate some degree of "partial deconfinement" of the Λ in the nuclear medium, which would manifest itself in terms of antisymmetrization corrections involving the non–strange quarks in the Λ. The resulting "Pauli pressure" could conceivably have some influence on deeply bound Λ levels. In practice, as we shall see, it is very difficult to separate such a quark effect from more conventional mechanisms which generate a non–local component of the Λ mean field (density dependence of the effective ΛN interaction, three–body forces, *etc.*).

In the past few years, there has been a slow but steady advance in the study of the production, spectroscopy and decays of strangeness $S = -1$ hypernuclei. Both the (π^+, K^+) and (K^-, π^-) reactions have been used to produce Λ hypernuclei. Because of their distinct momentum transfer characteristics, these processes are complementary, populating different parts of the hypernuclear spectrum. We discuss this in detail later. The $(K^-, \pi^-\gamma)$ reaction has been used to obtain precise energy splittings for a few *p*–shell hypernuclei. This enables one to obtain constraints on the spin dependence of the ΛN effective interaction. Both the spin–orbit and spin–spin parts of the ΛN force are found to be weak. The formation of Σ hypernuclei has been explored via the $(K^-, \pi^\pm)$ reactions, in experiments at CERN, Brookhaven and KEK. The existence of narrow Σ states is still a matter of considerable controversy. The non–mesonic weak process ΛN → NN has been accessed by measurements of the decays of hypernuclear ground states. The ratio of $\Lambda n \to nn$ and $\Lambda p \to np$ rates, as well as that for the Pauli–blocked Λ → Nπ mode, provide strong constraints on theoretical models. Existing meson exchange or hybrid (six–quark bag plus pion exchange) models do not explain the data. The reader is referred to a number of review papers on these topics: overviews have been given by Gal[1], Povh[2], Dalitz[3], and the present author[4]; data on $(K^-, \pi^-\gamma)$ is found in May *et al*[5], and interpreted by Millener *et al*[6]; measurements of Σ hypernuclear formation have been reported by Bertini *et al*[7], Piekarz *et al*[8], and Yamazaki *et al*[9], while a comprehensive review of Σ physics is found in Ref. 10. Recent weak decay measurements for hypernuclei are discussed by Grace *et al*[11], and a review of the theoretical problems has been given by Dover[12]. For a diverse view of a variety of topics in strange particle nuclear physics, the reader may also benefit from consulting the Proceedings of three recent conferences[13,14,15] in this area.

In the next few years, hypernuclear experiments will be focused on studies of K^- capture at rest[16] at KEK, leading to both Λ and Σ hypernuclear formation,

and studies of S = −1, −2 dibaryon production at the Brookhaven Alternating Gradient Synchrotron (AGS). The $K^- d \to \pi^- (\Lambda p)$ reaction has been frequently investigated[17], with a view towards finding narrow structures in the Λp invariant mass. Recent experiments at Brookhaven[18] have suggested a structure (in addition to the cusp phenomenon[19] at the ΣN threshold) near a mass of 2140 MeV/c^2. This object, call it D_t, is excited preferentially at larger momentum transfer q and hence is a phenomenon coupled to the p–wave ($L = 1$) of the Λp system. It would be tempting to associate this effect with the formation of a six–quark S = −1 dibaryon with $Q^4 \otimes Q^2$ ($L = 1$) structure (production cross sections in (K^-, π^-) were estimated in Ref. 20), but it may also be due to a conventional (meson exchange) final state interaction. The key question is whether D_t is a narrow state separated from the cusp phenomenon, or whether it represents simply a broadening of the cusp as q increases (as would be the case for a non–resonant but attractive p–wave final state interaction). The hypothesis of a narrow D_t has been defended in Ref. 18, but the analysis presented there is unconvincing. A further experiment[21] on the $^3\mathrm{He}(K^-, \pi^+)\Lambda nn$ reaction is approved for the AGS. Here, the prototype reaction is $K^- + (pp)_{^1S_0} \to \pi^+ + (\Lambda n)_{^1P_1}$, which would produce a spin singlet Λn dibaryon D_s. In six–quark bag calculations, the splitting of D_s and D_t is predicted[22] to be about 30 MeV, with D_s lying below D_t. Hints of the strange dibaryon structures D_s and D_t have also been seen[23] in the (p, K^+) reaction at SATURNE, but the purported peaks are mounted on a large quasifree background.

A new high momentum K^- beam line is under construction at the AGS, with the goal of producing S = −2 systems via the (K^-, K^+) double strangeness exchange reaction[24]. The first approved experiment for this new beam line is a search for the H dibaryon (a $J^\pi = 0^+$, $I = 0$, $uuddss$, $\mathrm{SU}(3)_f$ singlet six–quark object[25]). The proposal[26] is to produce a tagged Ξ^- beam via the $K^- p \to K^+ \Xi^-$ reaction, slow down and capture the Ξ^- in a deuterium target, and finally look for the mono–energetic neutron from the $\Xi^- d \to Hn$ process. Another experiment[27], involving the reaction $^3\mathrm{He}(K^-, K^+)Hn$, is also approved for the AGS.

There are numerous other possibilities for exploring the S = −2 sector via the (K^-, K^+) reaction. For instance, one could search for Ξ–hypernuclear states[28], since for some configurations the $\Xi^- p \to \Lambda\Lambda$ conversion width may be small. Also, the production of ΛΛ hypernuclei is an attractive possibility[29]; only two events are known[30] from emulsion studies.

In this introduction, I have tried to give some idea of the diverse nature of strange particle nuclear physics. Only a few selected topics will be treated in the following chapters, namely hypernuclear production mechanisms (Chap. 2), the example of ${}^{13}_{\Lambda}$C (Chap. 3), the phenomenology of the Λ mean field and its single particle energies (Chap. 4), and the "swelling" of nucleons in nucleus, as probed by K^+–nucleus scattering (Chap. 5). Some prospects for the future are discussed in Chap. 6.

2. PRODUCTION MECHANISMS FOR HYPERNUCLEI

Several reaction mechanisms have been used to produce hypernuclei. The most widely studied are the $(K^-, \pi^\pm)$ strangeness exchange and (π^+, K^+) associated production reactions, examined in detail below. One should also mention relativistic heavy ion collisions[31] and antiproton annihilation in nuclei[32]. Other processes, such as $(p, p'K^+)$ or (p, K^+), have also been investigated. At CEBAF, photoproduction of hypernuclei via (γ, K^+) or $(e, e'K^+)$ will be feasible.

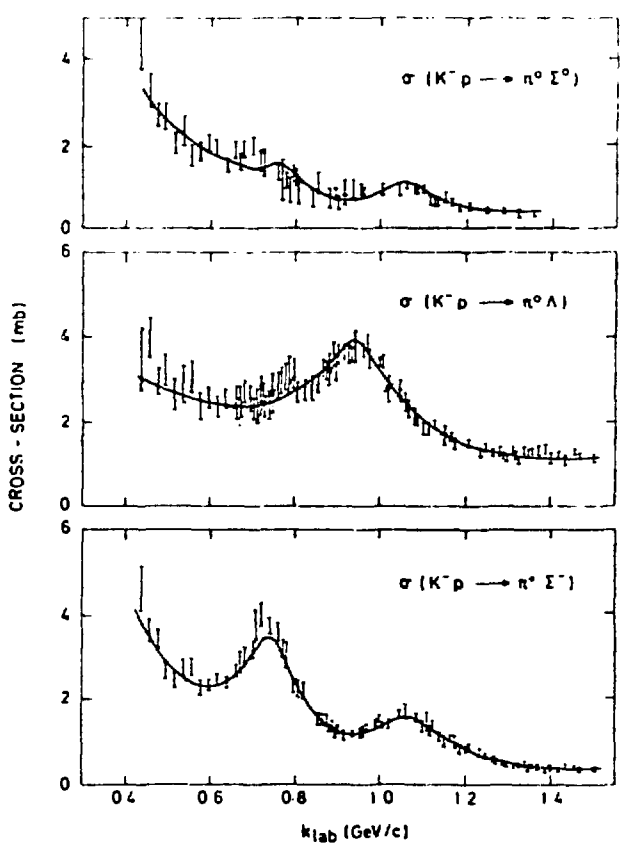

Fig. 1. Total cross sections for Λ or Σ production in K^-p collisions, as a function of lab momentum $k_{\rm lab}$ (from Ref. 33).

The K^-, unlike the K^+, can transfer one or two units of strangeness to a nucleon via reactions like $K^- + n \to \pi^- + \Lambda$ or $K^- + p \to K^+ + \Xi^-$. A pion, on the other hand, can stimulate the emission of an $s\bar{s}$ pair, leading to the process $\pi^+ + n \to K^+ + \Lambda$, for instance. The total cross sections[33] for Λ or Σ production with K^- beams are rather healthy, typically a few mb for K^- lab momenta in the range 600 – 800 MeV/c, as illustrated in Fig. 1. The 0^0 differential cross section $(d\sigma/d\Omega)_{0^0}$ for $K^-n \to \pi^-\Lambda$ near 800 MeV/c is about 4 – 5 mb/sr. For $\pi^+n \to K^+\Lambda$ associated production at peak, $(d\sigma/d\Omega)_{0^0}$ is about an order of magnitude smaller, as displayed[34] in Fig. 2. However, π^+ beam fluxes are much larger than for K^-, so the counting rate for a (π^+, K^+) run at the AGS actually exceeds that for a (K^-, π^-) experiment.

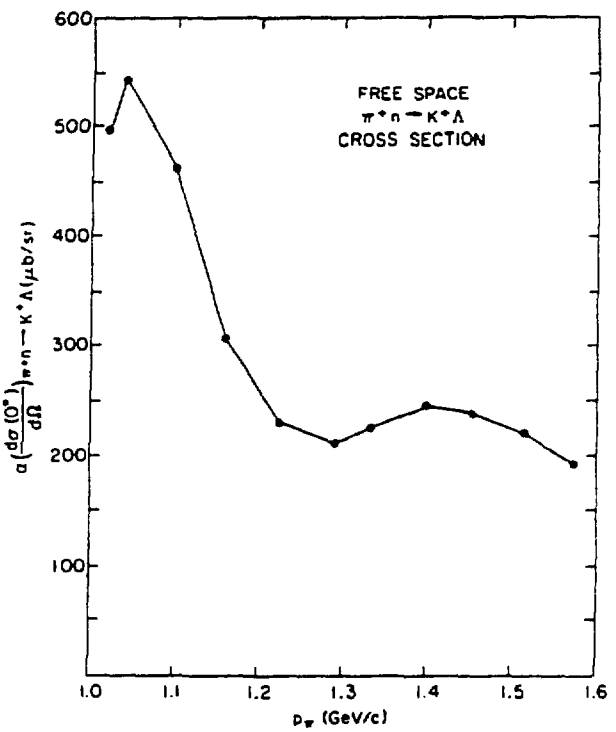

Fig. 2. Forward differential cross section for $\pi^+n \to K^+\Lambda$ as a function of pion lab momentum p_π (from Ref. 34).

The $K^-n \to \pi^-\Lambda$ and $\pi^+n \to K^+\Lambda$ reactions are kinematically quite distinct, as shown in Fig. 3. For the (K^-, π^-) reaction at 0°, there exists a "magic momentum" for the K^- at which the Λ or Σ is created at rest in the lab. The importance of this fact for hypernuclear production was first emphasized by Feshbach and Kerman[35], and exploited in the pioneering (K^-, π^-) experiments[36] at CERN. The Λ at rest has a sizable "sticking probability" for remaining bound

to the nucleus. The excitation of substitutional states, where the Λ occupies the same shell model orbit as was vacated by the nucleon, is highly favored in the (K^-, π^-) reaction near the "magic momentum" of 530 MeV/c. From Fig. 3, we see that $q\,(0°)$ remains small ($\leq$ 50 MeV/c) for $p_{K^-} \leq 800$ MeV/c.

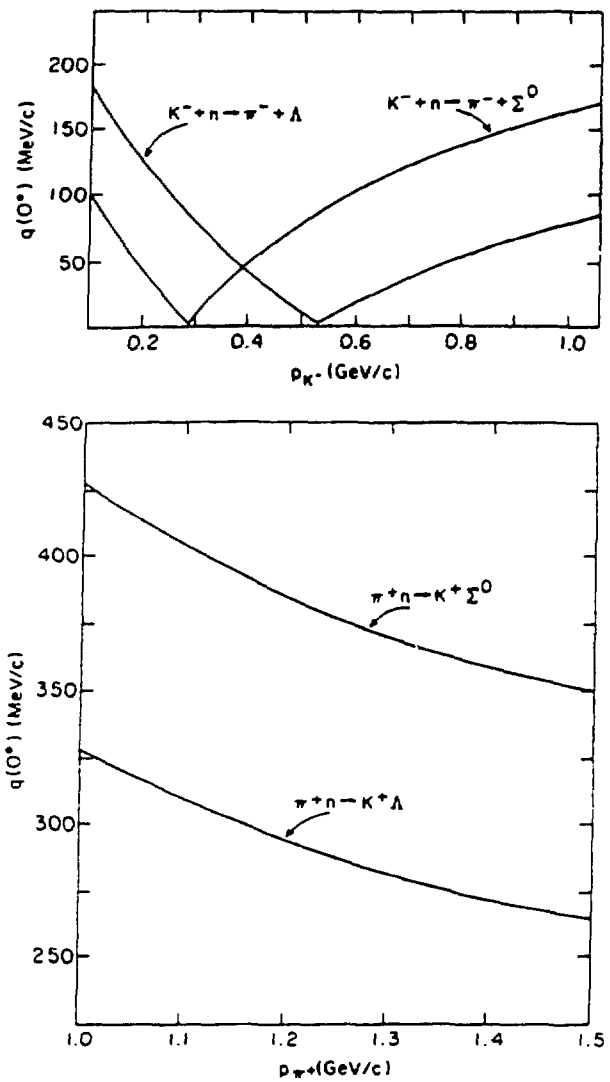

Fig. 3. Momentum transfer $q\,(0°)$ for (K^-, π^-) and (π^+, K^+) reactions as a function of lab momenta p_{K^-} or p_{π^+} (from Ref. 33).

The situation is quite different for the $\pi^+ n \rightarrow K^+\Lambda$ reaction. Here $q\,(0°) \geq p_F$, where $p_F = 270$ MeV/c is the Fermi momentum, for $p_{\pi^+} < 1.5$ GeV/c. The low spin states emphasized by the (K^-, π^-) process will be only weakly excited in (π^+, K^+). Rather, the (π^+, K^+) reaction excites high spin states. The selectivity for high spins will operate for $\gamma p \rightarrow K^+\Lambda$ and $K^- p \rightarrow K^+\Xi^-$ as well, where we also have $q\,(0°) > p_F$.

Let us quantify these remarks. For a 0^+ target, the differential cross section for the excitation of a pure Λ particle–neutron hole (ph) configuration of spin–parity J^π is given by

$$\frac{d\sigma}{d\Omega}\left(0^+ \to J^\pi\right) = \alpha\left(\frac{d\sigma}{d\Omega}\right)_{0^\circ} N_{\rm eff}^J \tag{1}$$

where $\alpha\,(d\sigma/d\Omega)_{0^\circ}$ is the $K^-n \to \pi^-\Lambda$ or $\pi^+n \to K^+\Lambda$ two–body cross section and $N_{\rm eff}^J$ is the effective neutron number given by

$$N_{\rm eff}^J = (2J+1)\ (2j_\Lambda+1)\ (2j_n+1)\ \begin{pmatrix} j_\Lambda & j_n & J \\ \frac{1}{2} & -\frac{1}{2} & 0 \end{pmatrix}^2 F(q) \tag{2}$$

where the form factor $F(q)$ in plane wave approximation (PWA) is defined by

$$F(q) = \left[\int_0^\infty r^2\, dr\, R_\Lambda(r)\ R_n(r)\ j_J(qr)\right]^2 \tag{3}$$

in terms of the radial wave functions R_Λ and R_n for the Λ and n single particle states $\{\ell_\Lambda,\ j_\Lambda\}$ and $\{\ell_n,\ j_n\}$. For $\left(K^-,\ \pi^-\right)$ and $\left(\pi^+,\ K^+\right)$, spin flip cross sections are negligible for small Θ, so only natural parity $\left(\pi = (-)^J\right)$ states will be populated. In $\left(e,\ e'K^+\right)$ or $\left(\gamma,\ K^+\right)$, on the other hand, spin flip states ($0^+ \to 1^+$, for example) are strongly excited[37].

For $\left(\pi^+,\ K^+\right)$, the "stretch" states with $J = \ell_\Lambda + \ell_n$ are kinematically favored. For nodeless $\{n,\ \Lambda\}$ oscillator "stretch" states, we have

$$F(q) = \frac{(2Z)^J\ e^{-Z}\ \left[\Gamma\left(J+3/2\right)\right]^2}{\left[(2J+1)!!\right]^2\ \Gamma\left(\ell_\Lambda+3/2\right)\ \ \Gamma\left(\ell_n+3/2\right)} \tag{4}$$

where $Z = (bq)^2/2$ and b is the radius parameter. Optimum kinematical matching occurs when $dF(q)/dq = 0$, or when

$$J = \frac{(bq)^2}{2} \tag{5}$$

We plot $F(q)$ in Fig. 4 for the $\left(1p_{3/2}^{-1}p_\Lambda\right)_{2^+}$ particle–hole configuration in ${}^{12}_{\Lambda}$C. The same $F(q)$ applies to $\left(K^-,\ \pi^-\right)$ and $\left(\pi^+,\ K^+\right)$ in PWA. We see that at $\theta_{\rm lab} = 0^\circ$,

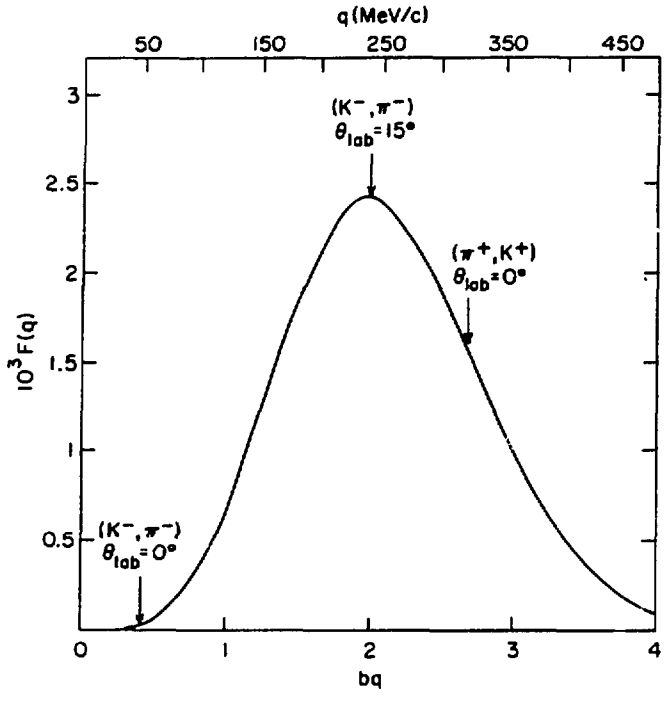

Fig. 4. The form factor $F(q)$ of Eq. (3) for excitation of the $\left(1p_{3/2}^{-1}\, 1p_\Lambda\right)_{2^+}$ configuration in ${}^{12}_{\Lambda}\mathrm{C}$ (from Ref. 34).

neither (K^-, π^-) or (π^+, K^+) is optimally matched, whereas for $\theta_{\rm lab} = 15°$, we hit the peak of $F(q)$ for the (K^-, π^-) reaction.

In Fig. 5, we plot J, as given by Eq. (5), as a function of target mass number A, using the parametrization

$$b \approx \frac{0.96A^{1/3}}{\left(1 - \frac{5}{9}A^{-1/3}\right)^{1/2}} \,. \tag{6}$$

For $p_\pi = 1.05$ GeV/c, there is good kinematic matching for the "leading trajectory" of high spin obtained by coupling the Λ in s_Λ, $p_\Lambda, d_\Lambda \ldots$ orbits to a neutron hole in the last valence shell. We return to this example in Chap. 5.

In (K^-, π^-) and (π^+, K^+) experiments done to date, the energy resolution ΔE has been in the range 2.5 – 6 MeV. With such coarse resolution experiments, one sees only the energy–averaged gross structure of hypernuclei, *i.e.*. the particle–hole structure. As an example, consider ${}^{16}_{\Lambda}\mathrm{O}$. The ground state doublet is $\left(p_{1/2}^{-1} \otimes s_{1/2}^{\Lambda}\right)_{0^-,1^-}$. The very small splitting of the doublet (estimated to be < 100 keV in Ref. 6) cannot be resolved experimentally, unless one measures the M1 γ–ray transition between the two levels, which has proved elusive. The low–lying natural parity excited states in ${}^{16}_{\Lambda}\mathrm{O}$ are

$$\left(p_{3/2}^{-1} \otimes s_{1/2}^{\Lambda}\right)_{1^-}, \; \left(p_{1/2}^{-1} \otimes p_{1/2,3/2}^{\Lambda}\right)_{0^+,2^+}, \; \left(p_{3/2}^{-1} \otimes p_{1/2,3/2}^{\Lambda}\right)_{0^+,\,2^+,2^+} \,. \tag{7}$$

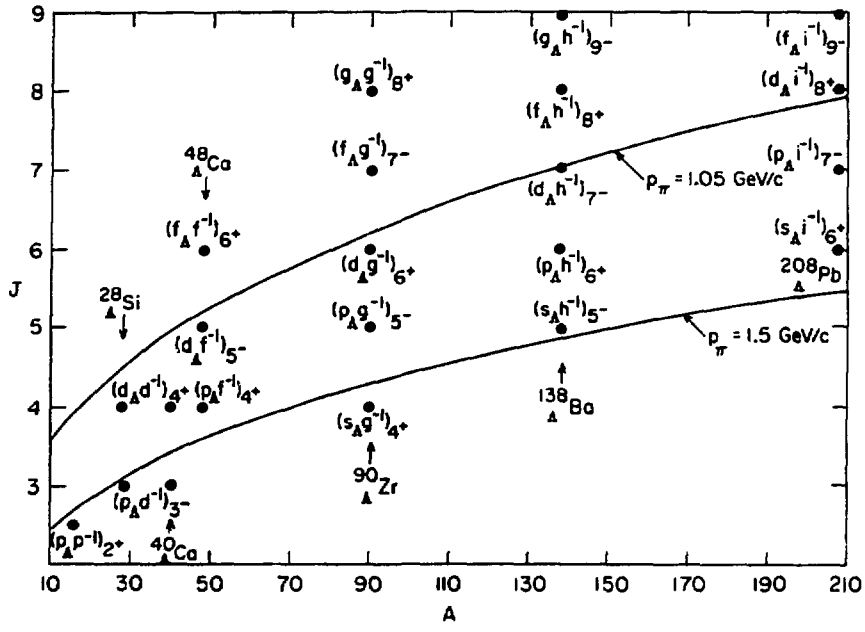

Fig. 5. Optimally matched J values (Eq. (5)) for $p_\pi = 1.05$ GeV/c and 1.5 GeV/c are shown as solid lines. Accessible natural parity "stretch" states with $J = \ell_\Lambda + \ell_n$ are indicated for several cases from $^{12}_{\Lambda}$C to $^{208}_{\Lambda}$Pb (from Ref. 4, Dover at Beijing).

The experimental excitation spectrum[36] for the (K^-, π^-) reaction on ^{16}O and ^{40}Ca targets at 0° is shown in Fig. 6. The spectrum displays peaks at energies corresponding to the $(0^+, 1^-)$ states of Eq. (7), as expected. The peaks corresponding to $\left(p_{1/2}^{-1} \otimes p_{1/2}^{\Lambda}\right)_{0^+}$ and $\left(p_{3/2}^{-1} \otimes p_{3/2}^{\Lambda}\right)_{0^+}$ are split in energy by about 6 MeV, which is just the nucleon spin–orbit splitting. This enables one to conclude that the Λ–nucleus spin–orbit potential is very small[2,36]. The interpretation of the $^{40}_{\Lambda}$Ca spectrum in Fig. 6 is similar: since $q\,(0°)$ is small, one is seeing the low spin $(0^+, 1^-)$ members of various Λn^{-1} configurations. The splitting of $\left(d_{3/2}^{-1} \otimes d_{3/2}^{\Lambda}\right)_{0^+}$ and $\left(d_{5/2}^{-1} \otimes d_{5/2}^{\Lambda}\right)_{0^+}$ states is again very close to the known nucleon spin–orbit splitting, indicating that spin–orbit effects are small for the Λ.

3. HYPERNUCLEAR STRUCTURE: THE EXAMPLE OF $^{13}_{\Lambda}$C

For closed shell 0^+ targets, the discussion of hypernuclear structure is naturally phrased in terms of particle–hole excitations, as discussed in Chap. 2. Here we examine the case of the ^{13}C$(K^-, \pi^-)^{13}_{\Lambda}$C reaction, where the spin of the target

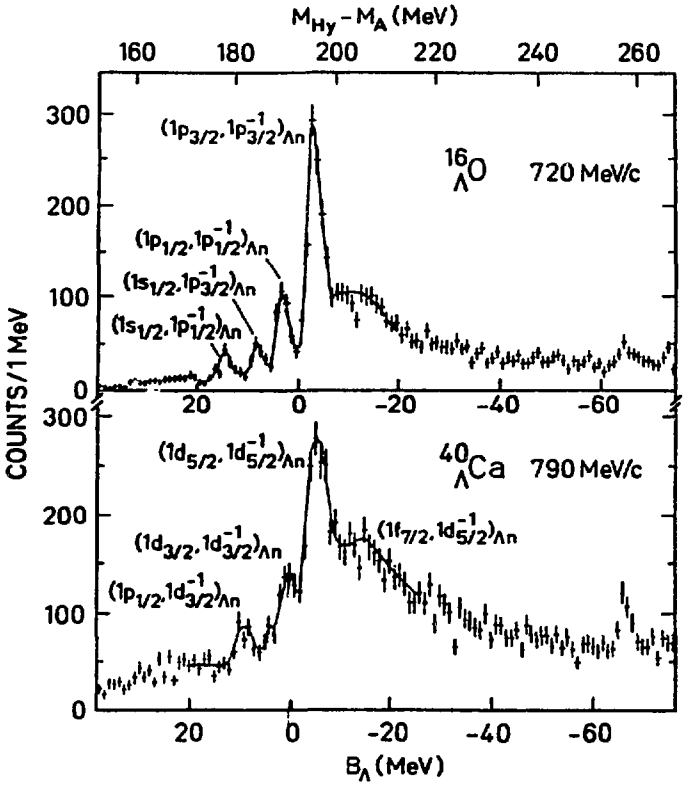

Fig. 6. Excitation spectrum for (K^-, π^-) on ^{16}O and ^{40}Ca targets at 0°, from Ref. 36.

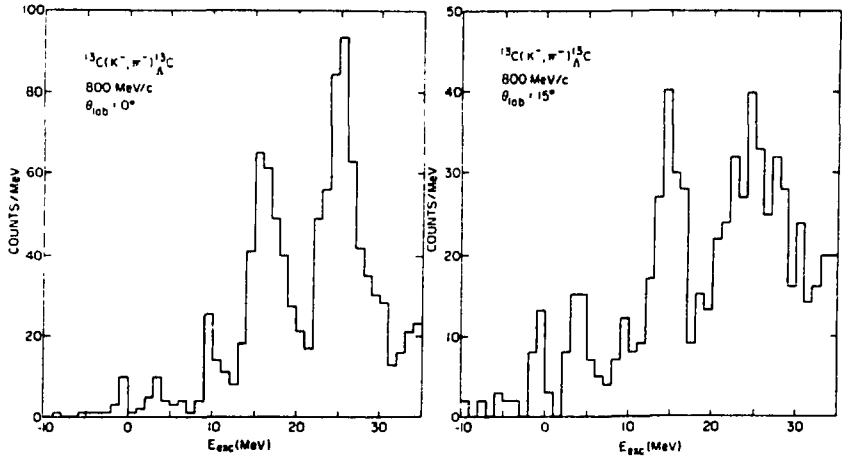

Fig. 7. Excitation spectrum for the $^{13}C(K^-, \pi^-)^{13}_{\Lambda}C$ reaction at 800 MeV/c, for lab angles $\theta_{lab} = 0°$, 15° (from Ref. 38).

leads to a greater richness of peaks, and some interesting constraints on the ΛN residual interaction emerge.

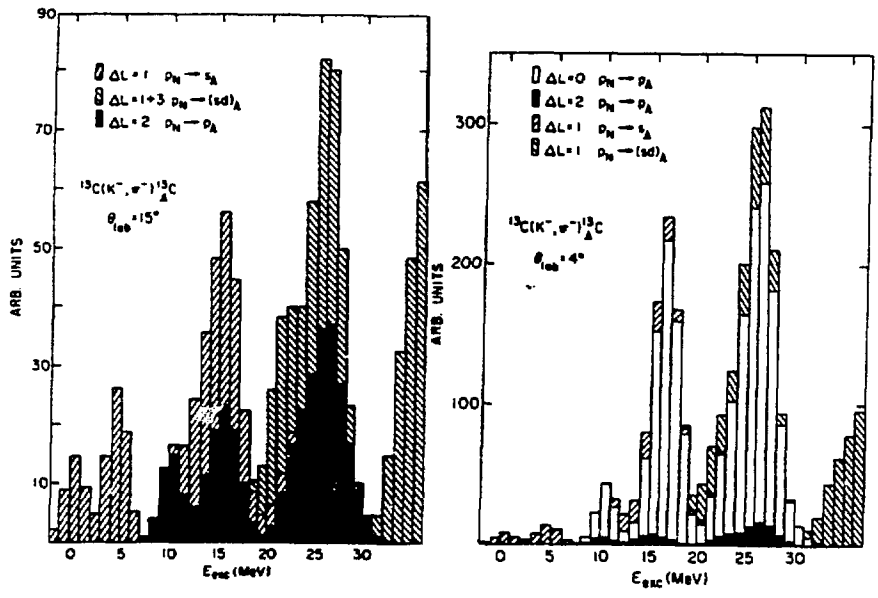

Fig. 8. Predicted spectrum for $^{13}\mathrm{C}(K^-, \pi^-)^{13}_{\Lambda}\mathrm{C}$ at 800 MeV/c, from Ref. 39.

The experimental spectrum of May *et al*[38] for $\theta_{\mathrm{lab}} = 0°$, 15° is shown in Fig. 7. The theoretical predictions[39], based on a shell model description of hypernuclear structure and a Distorted Wave Impulse Approximation (DWIA) for the (K^-, π^-) reaction mechanism, are shown in Fig. 8. The details of the theoretical framework are discussed below.

A comprehensive shell model for light hypernuclei, including core excitations and the effects of the ΛN residual interactions, was developed in Ref. 39. The calculations are done in the DWIA, using phenomenological Woods–Saxon optical potentials to generate the K^- and π^- distorted waves. The parameters of the potential are adjusted to fit the available K^- and π^- elastic scattering data on ^{12}C at the same momentum. A Fermi-averaged $K^-n \rightarrow \pi^-\Lambda$ amplitude in the lab system is used in the transition matrix element. Another ingredient is the choice of neutron and Λ bound state wave functions. These are generated from Woods–Saxon potentials whose geometry was chosen to be consistent with electron scattering charge distributions and neutron/proton single particle energies. Binding energies of (0.6, 0.1) MeV are used for the Λ in the $p_{3/2}$ and $p_{1/2}$ orbits, reflecting a small spin–orbit potential.

The differential (K^-, π^-) cross section for a transition $\alpha_i J_i T_i \rightarrow \alpha_f J_f T_f$ involving the single particle orbitals $\ell_N \rightarrow \ell_\Lambda$ is proportional to the sum

$$\sum_{\Delta L} \begin{pmatrix} \ell_N & \Delta L & \ell_\Lambda \\ 0 & 0 & 0 \end{pmatrix}^2 \left| M^{(\Delta L)}(q) \right|^2 \left(\alpha_f J_f T_f \left\| \left(a^\dagger_{\ell_\Lambda} \tilde{a}_{\ell_N} \right)^{\Delta L} \right\| \alpha_i J_i T_i \right)^2 \qquad (8)$$

where ΔL is the transferred angular momentum (spin flip is very small and has been neglected), and $M^{(\Delta L)}(q)$ are functions of momentum transfer q which result from the DWIA integration over distorted waves and an effective zero range amplitude for $K^- n \rightarrow \pi^- \Lambda$. The amplitudes $M^{(\Delta L)}(q)$ peak at different q values and lead to the excitation of distinct final states. $M^{(0)}(q)$, which excites $1/2^-$ states in ${}^{13}_{\Lambda}\mathrm{C}$ in $p_N \rightarrow p_\Lambda$ transitions, starting from the $1/2^-$ target ${}^{13}\mathrm{C}$, peaks at $\theta_L = 0°$. The $p_N \rightarrow s_\Lambda$ transition, driven by $M^{(1)}(q)$, leads to $1/2^+$ and $3/2^+$ final states, and peaks near $\theta_L = 10°$ for an 800 MeV/c incident momentum. Transitions $p_N \rightarrow p_\Lambda$ also receive a contribution from $M^{(2)}(q)$, which peaks near $\theta_L = 15°$ here and dominates $M^{(0)}(q)$ in this angular region; $M^{(2)}(q)$ populates $3/2^-$ and $5/2^-$ final states. The $5/2^+$ and $7/2^-$ states which arise in $p_N \rightarrow s_\Lambda$ and $p_N \rightarrow p_\Lambda$ transitions (involving the coupling of the Λ to a 2^+ core excited states of ${}^{12}\mathrm{C}$) involve spin flip ($\Delta S = 1$) for their excitation, and are produced only very weakly in the (K^-, π^-) reaction.

The predicted cross sections in Fig. 8 are binned as in the experiment to facilitate comparison. The contributions of each ΔL are shown separately, and display the qualitative features just discussed. The agreement of the DWIA theory and the data is very good, both in angular shapes (not shown) and absolute cross sections. This gives confidence in our theory of the reaction mechanism and the resulting spin assignments.

We now discuss the detailed spectroscopy of ${}^{13}_{\Lambda}\mathrm{C}$. Some of the main features, in particular rough estimates of the energies and relative intensities of the dominant peaks, already emerge from a weak coupling picture (but, as we see later, there are important changes in some cases from residual ΛN interactions). Core excited states in ${}^{12}\mathrm{C}$ play a crucial role in the interpretation: besides the 0^+ $(T = 0)$ ground state of ${}^{12}\mathrm{C}$, strong excitations in ${}^{13}_{\Lambda}\mathrm{C}$ are seen in which the Λ couples to the 2^+ $(T = 0)$, 1^+ $(T = 0)$, 1^+ $(T = 1)$ and 2^+ $(T = 1)$ excited states of ${}^{12}\mathrm{C}$ at 4.4, 12.7, 15.1 and 16.1 MeV, respectively. In weak coupling, the entire (K^-, π^-) cross section associated with a given core state is proportional to the neutron pickup

strength, known from the reaction $^{13}C(p,d)\ ^{12}C^*$. A poor resolution experiment, which sums over groups of final states, sees just this strength.

The $\Delta L = 1$ strength seen around excitation energy 0 and $4-5$ MeV corresponds to the $1/2^+$ ground state and a $3/2^+$ state obtained by coupling the $s_{1/2}$ Λ to the ^{12}C ground state and 2^+ $(T=0)$ state at 4.4 MeV, respectively. The peak around 10 MeV is due to $p_N \rightarrow p_\Lambda$ transitions; for $\theta_L = 0°$ and 15°, the $1/2^-$ and $3/2^-$ states, respectively, obtained by coupling ${}_\Lambda p_{1/2}$ and ${}_\Lambda p_{3/2}$ to the 0^+ ground state of ^{12}C, dominate the cross section. As we show later, the energy shift of the 10 MeV state between 0° and 15° offers a constraint on the Λ spin–orbit interaction. Between 12 and 16 MeV of excitation energy, one sees several positive parity $(1/2^+,\ 3/2^+)$ states obtained by coupling ${}_\Lambda s_{1/2}$ to core excited states of ^{12}C. The $3/2^+$ states represent a significant fraction of the strength in the 16 MeV peak at 15°. The rest of the 16 MeV strength is mostly due to two $5/2^-$ states $(\Delta L = 2)$ obtained by coupling ${}_\Lambda p_{1/2,3/2}$ to the 2^+ $(T=0)$ core state at 4.4 MeV. At 4°, in contrast, the $1/2^-$ from ${}_\Lambda p_{3/2}$ coupled to 2^+ $(T=0)$ is dominant $(\Delta L = 0)$. The 25 MeV peak encompasses many states arising from the coupling of ${}_\Lambda p_{1/2,3/2}$ to core states in the $13-16$ MeV excitation region in ^{12}C. At 0°, $\Delta L = 0$ is largest, and we see mostly $1/2^-$ states from ${}_\Lambda p_{3/2}$ coupled to $J^\pi = 1^+$ and 2^+ cores. At 15°, the $3/2^-$ and $5/2^-$ members are seen via $\Delta L = 2$, but there are also sizable contributions from $p_N \rightarrow (sd)_\Lambda$ transitions with $\Delta L = 1,\ 3$.

The interesting physics of $^{13}_{\Lambda}C$ is revealed in the deviations of the energies and relative intensities from the naive weak coupling picture. These differences are generated by the ΛN residual interaction $V_{\Lambda N}$, which we take to have the phenomenological form

$$\begin{aligned} V_{\Lambda N}\left(\underset{\sim}{r}_N - \underset{\sim}{r}_\Lambda\right) &= V_0\left(\underset{\sim}{r}_N - \underset{\sim}{r}_\Lambda\right)\ (1 - \in + \in P_x)\ \left(1 + \alpha \underset{\sim}{\sigma}_N \cdot \underset{\sim}{\sigma}_\Lambda\right) \\ &\quad + V_\pm\left(\underset{\sim}{r}_N - \underset{\sim}{r}_\Lambda\right)\ \left(\underset{\sim}{\sigma}_\Lambda \pm \underset{\sim}{\sigma}_N\right)\ \cdot \underset{\sim}{\ell}_{N\Lambda}\ . \end{aligned} \tag{9}$$

In addition to two–body symmetric and antisymmetric spin–orbit potentials $V_\pm$, we have introduced a one–body spin–orbit term for the Λ. We expand the central part

$$V_0\left(\underset{\sim}{r}_N - \underset{\sim}{r}_\Lambda\right) = \sum_{k=0}^{\infty} V_k\left(r_N,\ r_\Lambda\right) P_k\left(\cos\theta_{\underset{\sim}{r}_N,\ \underset{\sim}{r}_\Lambda}\right)\ . \tag{10}$$

and define the usual Slater integrals

$$F^{(k)} = \int R^2_{\ell_N}\left(r_N\right)\ \ R^2_{\ell_\Lambda}\left(r_\Lambda\right)\ \ V_k\left(r_N, R_\Lambda\right)\ dr_N\, dr_\Lambda\ . \tag{11}$$

For $\ell_N = 1$, $\ell_\Lambda = 1$ we have only $F^{(0)}$ and $F^{(2)}$; the latter reflects the quadrupole part of the ΛN potential. The spin–orbit potential gives rise to a splitting $\in_{p^\Lambda_{1/2}} - \in_{p^\Lambda_{3/2}} = \in_p$. We assume $F^{(0)} = -1.16$ MeV, $\alpha = -0.1$, $\in = 0$ and study the $^{13}_{\Lambda}$C spectrum as a function of $F^{(2)}$ and $\in_p$. The energy differences of the observed peaks differ from naive predictions based only on the energies of core states, allowing us to constrain $\in_p$ and $F^{(2)}$.

In the absence of an interaction of $\underset{\sim}{\sigma}_\Lambda$ with the nuclear core, the lowest $1/2^-$ and $3/2^-$ states of $^{13}_{\Lambda}$C, obtained mainly by coupling ${}_\Lambda p_{1/2,3/2}$ to the 0^+ ground state of ^{12}C, would be degenerate. Independent of $F^{(2)}$, the small shift[38] $\Delta E = 0.36 \pm 0.3$ MeV in the 10 MeV peak between 0° ($1/2^-$ dominant), and 15° ($3/2^-$) constrains the combination of one and two–body spin–orbit potentials to be small. If we choose $V_\pm = 0$, a value $\in_p \approx 0.5$ MeV is likely, while if we use a pure two–body spin–orbit force, a slightly larger $\in_p$ is favored. This example provides a particularly clean test of the Λ spin–orbit strength. These conclusions are consistent with those of the CERN group based on $^{16}_{\Lambda}$O, i.e., the Λ spin–orbit strength is very small but likely of the same sign as that for the nucleon. A better value for the Λ spin–orbit coupling is in principle obtainable from the $(K^-, \pi^-\gamma)$ reaction. The E1 γ–rays from the $1/2^-$ and $3/2^-$ levels lead to the ground state of $^{13}_{\Lambda}$C, but with isotropic and $1 - 0.6\cos^2\theta$ angular distributions[40], respectively.

Using $\in_p = 0.5$ MeV, $V_\pm = 0$, we may now use other energy differences to constrain $F^{(2)}$. The shift $\Delta E = 1.7 \pm 0.4$ MeV of the 16 MeV peak between 0° and 15°, if we subtract the $p_N \rightarrow s_\Lambda$ strength, yields a $1/2^- - 5/2^-$ splitting (same 2^+ $(T = 0)$ core state) generated by $F^{(2)}$. The splitting of the 16 and 25 MeV peaks at 0°, both dominated by $1/2^-$ states with ${}_\Lambda p_{3/2}$, is less (9.3 MeV) than the naive estimate of 11.7 MeV based on the 2^+ $(T = 0)$ and 2^+ $(T = 1)$ core states. This is also due to $F^{(2)}$. In both cases, the data can be accounted for by using -3.4 MeV $< F^{(2)} < -3$ MeV; this value is close to the value of $F^{(2)}$ extracted from the 0° $^{9}_{\Lambda}$Be spectrum by Dalitz and Gal[41].

The most interesting aspects of the $^{13}_{\Lambda}$C spectrum are the energy splitting ΔE and intensity ratio R of the 16 and 10 MeV peaks at 0°. Here, the weak coupling basis states $|0^+ (T = 0) \otimes {}_\Lambda p_{1/2}\rangle_{1/2^-}$ and $|2^+ (T = 0) \otimes {}_\Lambda p_{3/2}\rangle_{1/2^-}$ are significantly mixed by $F^{(2)}$. If we write

$$\left|1/2^- >_1 = \alpha \left|0^+ \otimes {}_\Lambda p_{1/2} > - \beta \right| 2^+ \otimes {}_\Lambda p_{3/2} > , \qquad (12)$$

then

$$R = \frac{(\beta\theta(1/2) + \alpha\theta(3/2))^2}{(\alpha\theta(1/2) - \beta\theta(3/2))^2}\ , \tag{13}$$

where $\theta(1/2)$ and $\theta(3/2)$ are the spectroscopic amplitudes for neutron pickup from the ^{13}C ground state to the first 0^+ and 2^+ states of ^{12}C, respectively. With no mixing, and using Cohen–Kurath wave functions[42], one obtains $R = 1.8$. The experimental value[38] is $R \approx 5$, while the theoretical values one obtains with mixing ($\alpha \approx 0.96, \beta \approx 0.28$, $F_2 \approx -3$ to -3.5 MeV) are $R \approx 6 - 7$. If one makes $\in$ too large, R increases to unacceptably large values.

Despite the relatively weak ΛN force, the hypernucleus displays a tendency to seek a higher degree of spatial symmetry in the lowest $1/2^-$ state. If instead of the weak coupling basis, we used the states of [54] and [441] symmetry, the first $1/2^-$ is dominantly the [54] symmetry, which is forbidden by the Pauli principle for a system of nucleons. In the limit where [54] symmetry is exact for this $1/2^-$ state, one has a dynamical selection rule inhibiting its population in the (K^-, π^-) reaction, since a [54] symmetry is unreachable with $\Delta L = 0$, starting with the dominant [441] of the ^{13}C ground state. This tendency towards spatial symmetry (increased by using $\in > 0$) accounts for the strong deviation of R from its pickup value in the weak coupling limit.

The full exploitation of the structure information available from Λ–hypernuclear spectra clearly requires a considerable improvement in energy resolution, available only with more intense K^- beams. As indicated here, however, one already obtains non–trivial constraints on $\in_p$ and $F^{(2)}$ from the coarse resolution data.

4. PHENOMENOLOGY OF Λ SINGLE PARTICLE ENERGIES

Recently, a Brookhaven - LANL - Houston - Tohoku - TRIUMF - Vassar - CMU - FSU - Mississippi collaboration has measured[43] (π^+, K^+) cross sections on ^{9}Be, ^{12}C, ^{13}C, ^{16}O, ^{28}Si, ^{40}Ca, ^{51}V, and ^{89}Y targets at $p_\pi = 1.05$ GeV/c. These represent the first data for heavy targets, and enable us to track the evolution of Λ single particle binding energies as a function of A. The preliminary data for $^{89}\mathrm{Y}(\pi^+, K^+)^{89}_{\Lambda}\mathrm{Y}$ are shown in Fig. 9. One observes a series of rather sharp peaks on a smoothly rising background. We identify these peaks with the s_Λ, p_Λ, d_Λ,

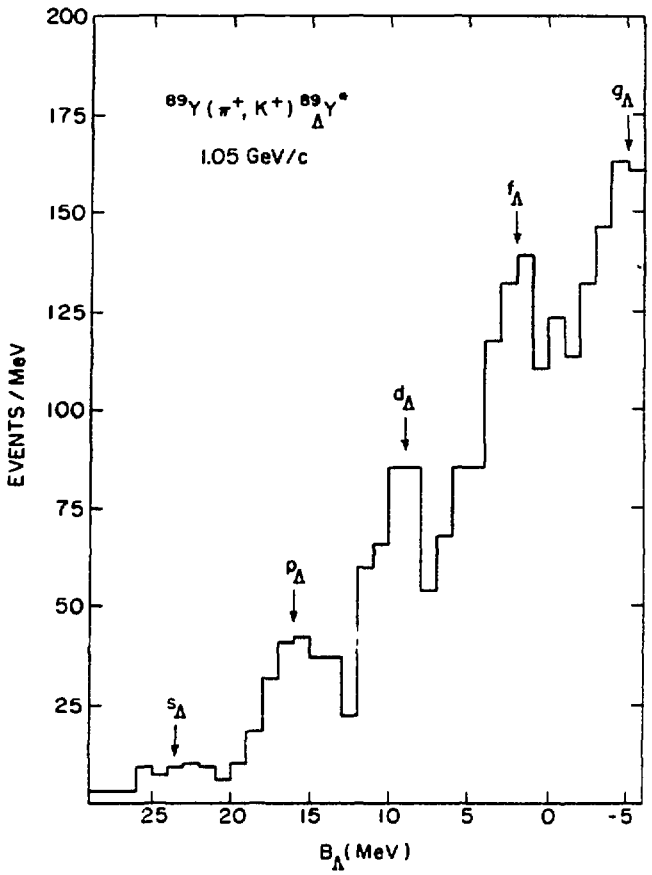

Fig. 9. The excitation spectrum of the $^{89}_{\Lambda}$Y hypernucleus, as produced in the (π^+, K^+) reaction at 1.05 GeV/c. The data are taken from Ref. 43. The labels $\{s_\Lambda, p_\Lambda, d_\Lambda, f_\Lambda, g_\Lambda\}$ identify the values of binding energy B_Λ predicted in Ref. 34 based on a Woods–Saxon potential for the Λ.

and f_Λ bound states of the Λ. The arrows in Fig. 9 indicate the orbital angular momenta assigned to these states.

Note that the nodeless g_Λ state is predicted[34] to lie about 5 MeV in the continuum near $A = 90$, with an elastic width of about 900 keV, and may be visible in the data. This width is small because of the relatively large ℓ_Λ of the state. The existence of a narrow single particle Λ resonance in the continuum is not specific to the mass 90 region. Narrow states ($1d_\Lambda$ in $^{28}_{\Lambda}$Si, $1h_\Lambda$ in $^{138}_{\Lambda}$Ba, $1i_\Lambda$ in $^{208}_{\Lambda}$Pb, for instance) with elastic widths of 1 MeV or less are predicted throughout the periodic table.

In addition to the (π^+, K^+) data, emulsion studies[44] provide accurate values for s_Λ binding energies in light nuclei and upper limits on B_Λ for medium mass nuclei[45]. More recently, (K^-, π^-) reaction studies[46] have yielded binding energy data for $^{12}_{\Lambda}$C, $^{27}_{\Lambda}$Al, $^{32}_{\Lambda}$S, $^{40}_{\Lambda}$Ca, $^{51}_{\Lambda}$V and $^{209}_{\Lambda}$Bi.

The B_Λ data can be reasonably well fit with a Woods–Saxon potential of depth around 30 MeV, about $1/2$ of that for the nucleon. The new (π^+, K^+)

data provide the level spacings in a given hypernucleus (see Fig. 9), so one can determine more about the geometry of the Λ–nucleus potential. We outline here a description[47] based on the Skyrme–Hartree–Fock (SHF) approach[48], first applied to hypernuclei by Rayet[49]. We replace the non–local Λ–nucleus interaction by an energy–dependent local potential $V(r, E)$ of the form

$$
\begin{aligned}
V(r, E) &= \frac{m_\Lambda^*(r)}{m_\Lambda} U(r) + \left(1 - \frac{m_\Lambda^*(r)}{m_\Lambda}\right) E \\
U(r) &= \tilde{t}_0 \rho(r) + \frac{3}{8} t_3 \rho^2(r) + \frac{1}{4}(t_1 + t_2)\, T(r) \qquad (14) \\
T(r) &= \frac{3}{5}\left(\frac{3}{2}\pi^2\right)^{2/3} \rho^{5/3}(r) \\
\frac{\hbar^2}{2m_\Lambda^*(r)} &= \frac{\hbar^2}{2m_\Lambda} + \frac{1}{4}(t_1 + t_2)\, \rho(r) \ .
\end{aligned}
$$

Here m_Λ is the free space Λ mass and $m_\Lambda^*(r)$ is the effective Λ mass in the nuclear medium of density $\rho(r)$. We have set N = Z and neglected derivatives of the density. We shall use densities which are proportional to the empirically determined charge densities. From Eq. (14), we see that there are three parameters in the model: $\tilde{t}_0$, $t_1 + t_2$, and t_3. We retain the standard SHF parametrization[50] to facilitate the comparison of Λ–nucleus and nucleon–nucleus potentials.

The term linear in density in $U(r)$ results from folding the density–independent part of the ΛN effective interaction with the point nucleon density. The resultant potential well[51] has increased diffusivity and a slightly smaller half–density radius.

The ρ^2 term in Eq. (14) may arise from the density dependence of the ΛN interaction[52], as would be the case for Skyrme models[49], or from certain forms of ΛNN three–body interactions[53], or perhaps quark rearrangement effects[54]. This term need not be quadratic in form. The essential point is that a repulsive ρ^γ term, with $\gamma > 1$, leads to a potential with an increased central radius[51], a surface effect which is independent of A. Clearly, a fixed increase in the radius increases the effective radius parameter r_0 for light nuclei relative to r_0 for heavy nuclei. This mechanism explains the difference in radii between the potential and the underlying density.

Since the energy levels in a non–local potential are spread out by the energy–dependent term in the equivalent local potential of Eq. (14), a simultaneous description of B_Λ in ${}^{16}_{\Lambda}$O and ${}^{89}_{\Lambda}$Y is achievable. The $t_3\,\rho^2(r)$ term can be used to adjust the radius of the well to fit ${}^{16}_{\Lambda}$O, while the $(1 - m_\Lambda^*(r)/m_\Lambda)\, E$ term can be used

to counteract the compression of the ${}^{89}_{\Lambda}$Y spectrum. The choice of parameters[47] $\tilde{t}_0 = -402.6$ MeV $\cdot$ fm^3, $t_3 = 3394.6$ MeV $\cdot$ fm^6, $t_1 + t_2 = 103.44$ MeV $\cdot$ fm^5 gives an excellent fit to all the existing B_Λ data, as shown in Fig. 10. These values correspond to an effective mass $m^*_\Lambda(0)/m_\Lambda \approx 0.8$ in the interior of the hypernucleus, and a Λ well depth of $D_\Lambda \approx 27.5$ MeV. In the SHF approach, m^*_Λ/m_Λ and D_Λ are rather tightly constrained if one requires a simultaneous fit to level spacings for both light and heavy hypernuclei.

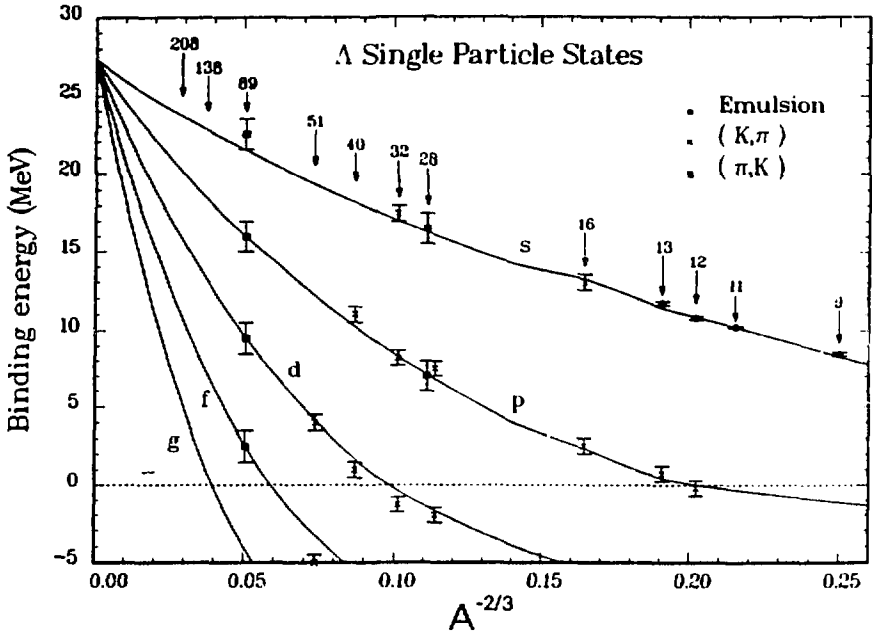

Fig. 10. Experimental binding energies (dots, crosses, squares) for s, p, d, f single particle states of the Λ as a function of $A^{-2/3}$ (A = mass number of core). The solid curves represent a best fit with the SHF form (14) for the Λ potential[47].

Let us now compare with some qualitative features of SHF for nucleon orbits. If $t_3 = 0$, nucleon level spacings are far too large, so a substantial $t_3\,\rho^2(r)$ term is required[48,50]. However, within the Skyrme model, it is not possible to simultaneously describe the nucleon level density at the Fermi surface (which requires $m^*_N/m_N \approx 1$) and the deeply bound levels (which need $m^*_N/m_N \approx 1/2$). In contrast, for the more weakly interacting, distinguishable Λ, an excellent description[47] of the B_Λ values, from the most deeply bound states to unbound resonances, is possible with a single value of m^*_Λ/m_Λ.

Recently, a number of attempts have been made to calculate the Λ–nucleus potential starting from a free space ΛN interaction[52,55–57]. Yamamoto and Bandō[52] obtain a value of D_Λ consistent with the empirical value, and an effective mass $m^*_\Lambda/m_\Lambda \approx 0.78$. Refinements in the construction of Λ–nucleus potentials have been made by Yamamoto[56] and Kohno[57]. The general features of the Λ–nucleus potential obtained from the free ΛN interaction seem to be consistent with those we have obtained[47] from a rather precise fit to the binding energies of Λ single particle levels.

The Λ–nucleus spectrum provides a "textbook" example of single particle structure in nuclear physics. In ordinary nuclei, single particle strength rapidly becomes fragmented with increasing excitation energy, and the deeply bound hole states become so broad as to be essentially unobservable. Even in the region of the Fermi surface, where excellent examples of the basic single particle structure abound, coupling to vibrational states of the core is important and leads to an apparent compression of the single particle spectrum. In the hypernuclear case, the fact that the Λ is a distinguishable particle, which interacts rather weakly with the nuclear core, leads to a clearly defined set of single particle states. These states can be thought of as doorway states which acquire a spreading width by mixing with a dense background of hypernuclear levels. An estimation of these widths, together with escape widths (e.g. for proton emission) will be necessary to understand the widths of the peaks observed in the (π^+, K^+) reaction on heavy targets. The observed peaks in Fig. 9 are certainly broader than the experimental resolution. The widths of the peaks will limit the largest mass number for which the Λ single particle structure can be investigated, at least with the present resolution of about 3 MeV, since the intershell spacing will eventually become comparable with the width. However, it should be possible to investigate the structure $\left(h^{-1}_{11/2}\ell_\Lambda\right)$ for a ^{138}Ba target.

The discussion thus far has not made reference to the role of quarks. The differences between the Λ and N spectra hinge on several factors:

1) The non–locality of the self–consistent field (*i.e.*, the choice of t_1 and t_2). The differences between Λ and N largely reflect the range of the effective interaction, which is larger for NN than for ΛN because of the role of the π exchange Fock term for the former. This is a non–perturbative long–range effect having nothing to do with short–range quark properties.

2) The role of $t_3\,\rho^2\,(r)$ terms. These are a complicated mixture of density–dependent modifications of the two–body interaction and perhaps genuine three–body interactions. It has been proposed that the "Pauli pressure" due to quark antisymmetrization[54,58] generates an effective ΔNN force. However, it is difficult to separate this subtle effect from more conventional $\rho^2\,(r)$ terms which arise from long–range effects. Effects of partial deconfinement of strange quarks in the nucleus, or the possibility of an increased size for hyperons[59] relative to nucleons (even in free space) are intriguing, but such signatures of the quark degrees of freedom cannot be isolated in a convincing way from the data. The level spectra are consistent with the picture of the Λ as a distinguishable baryon.

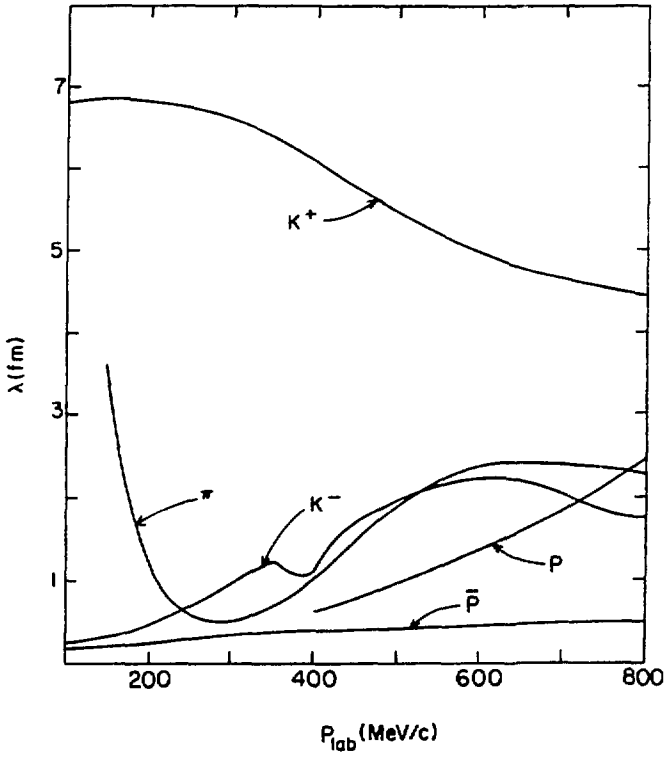

Fig. 11. Mean free path λ of various hadrons in nuclear matter (from Ref. 33).

5. K^+–NUCLEUS SCATTERING AND THE "SWELLING" OF NUCLEONS IN NUCLEI

The K^+–nucleon interaction below 300 MeV/c is dominated by the $I = 1$ s–wave (S_{11}) amplitude. We have $\delta\,(S_{11}) = -kR$, where $R \approx 0.32$ fm. This rather modest phase shift generates only a small total K^+N cross section (< 10 mb for $p_{\rm lab} <$

400 MeV) and hence the mean free path λ of a K^+ is rather long at low $p_{\rm lab}$, as shown in Fig. 11. Among other hadrons, only the pion (at very small momentum) has such a large λ. Thus, the K^+ serves as a volume probe of nuclei, and is sensitive to density dependent "swelling" phenomena which are most significant in the nuclear interior. For a strongly absorbed probe such as the K^-, on the other hand, there is considerable multiple scattering in nuclei, and hence "shadowing" is observed in K^+–nucleus total cross sections (i.e., $\sigma_T\,(K^- + A) \;< A\,\sigma_T\,(K^-\mathrm{N})$). This is clearly observed in Fig. 12. For K^+, the multiple scattering is minimal; in fact, for $p_{\rm lab} < 1$ GeV or so, K^+–nucleus cross sections exhibit "antishadowing" (see Fig. 12). At higher momenta, for which the K^+N cross section approaches normal hadronic size, "shadowing" is observed.

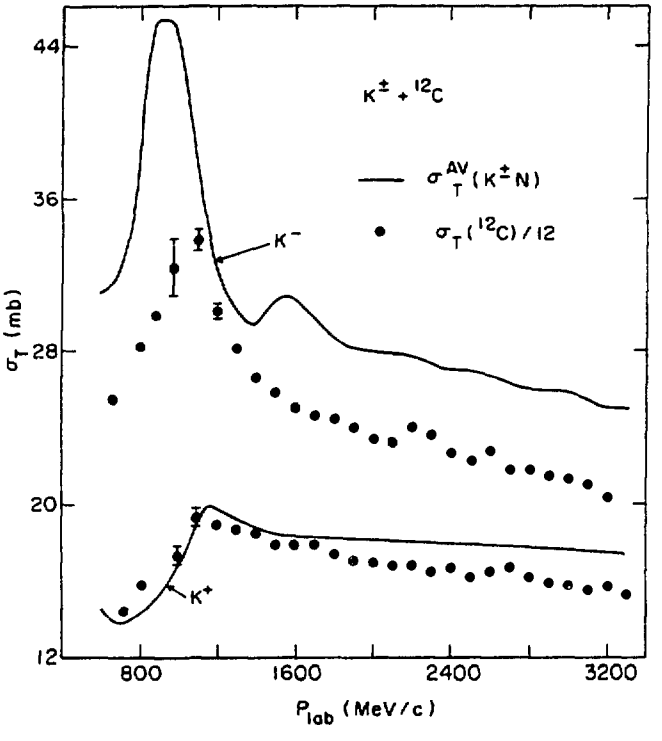

Fig. 12. Total cross sections per nucleon for $K^\pm + {}^{12}C$ (dots), compared to the $K^\pm$N cross sections (solid lines), taken from Ref. 33.

In meson–exchange models of the K^+N interaction, vector mesons play a significant role, since single pion exchange is not allowed. In the nuclear medium, the vector meson mass $m_V\,(\rho)$ depends on the density ρ, and hence the effective

amplitude $f_{K^+N}(\rho)$ also becomes density dependent. Brown *et al*[60] have developed a simple model for $f_{K^+N}(\rho)$. They write in Born approximation

$$f_{K^+N}(\rho) = \frac{f_{K^+N}(0)}{\left(1 - \frac{\lambda\rho}{2\rho_0}\right)^2} \tag{15}$$

where $\rho_0 \approx 1/6$ fm^{-3} in the density of nuclear matter, and λ is a constant which has been estimated in several ways[60], for instance

$$\lambda \approx 2\left[1 - \frac{m_N(\rho_0)}{m_N(0)}\right] \tag{16}$$

in terms of the density–dependent nucleon–effective mass $m_N(\rho)$. This gives $\lambda \approx 0.2 - 0.3$. From Eq. (15), one can construct the K^+–nucleus optical potential

$$V_{opt}^{K^+}(r) = V_0^{K^+} \frac{\rho(r)/\rho_0}{1 - \lambda\,\rho(r)/\rho_0} \approx \frac{\tilde{V}_0^{K^+}}{1 + e^{(r-\tilde{R})/\tilde{a}}}, \tag{17}$$

where $V_0^{K^+} = -2\pi f_{K^+N}(0)\ \rho_0/E_{K^+}$ and $\tilde{V}_0^{K^+} = V_0^{K^+}/(1-\lambda)$. The effect of the non–linear density dependence in Eq. (17) is an increased repulsion in the K^+ real potential and a decreased effective radius $\tilde{R} = R - \lambda a$ for the nucleus ($\{R, a\}$ are the usual radius and diffuseness parameters of a Woods–Saxon potential). This is exactly what was needed in previous phenomenological fits[61,62] to the $K^+ + {}^{12}C$ elastic scattering data at 800 MeV/c.

The results of an optical model calculation for $K^+ + {}^{12}C$ utilizing Eq. (17) are shown in Fig. 13 for $\lambda = 0, 0.2$. The elastic data are from Marlow *et al*[61], and the total cross sections are due to Bugg *et al*[63]. The choice $\lambda = 0.2$, consistent with Eq. (16), gives a good fit to the data, whereas the choice $\lambda = 0$ (free K^+N amplitudes) is inadequate.

In the preceding discussion, we have assumed that the ρ– and ω–exchange contributions to f_{K^+N} are subject to the same density–dependent renormalization. Note that $K^+ + {}^{12}C$ elastic scattering involves the isospin–averaged K^+N amplitude, so that the ρ cancels out in Born approximation, and only ω enters. Both the ρ and ω contribute in first order, however, to $(K^+, K^{+\prime}N)$ quasifree scattering, which constitutes the bulk of the total cross section at 800 MeV/c. In the (K^+, K^0) charge–exchange process, on the other hand, only the ρ contributes in first order. Experimentally, separate measurements of K^+ elastic, charge–exchange, and total–reaction cross sections on light targets as functions of p_L

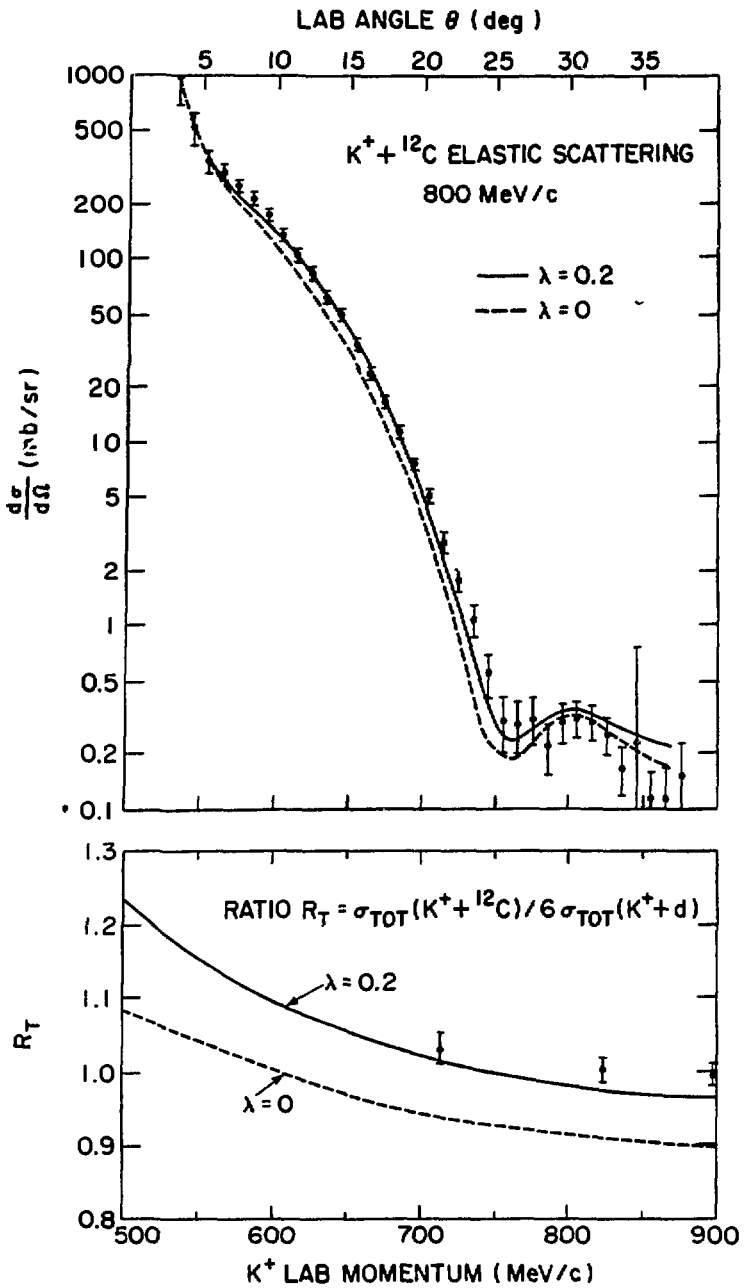

Fig. 13. Angular distribution for $K^+ + {}^{12}C$ elastic scattering at 800 MeV/c (top); the elastic data are from Marlow *et al*[61]. The ratio $R_T = \sigma_T\,(K^+ + {}^{12}C)\ /\ 6\sigma_T\,(K^+ + d)$ is shown at the bottom; the σ_T data are from Bugg *et al*[63]. The dashed and solid curves represent optical model calculations[60] using the K^+ potential of Eq. (17).

would be an invaluable aid to disentangling the isospin structure of the process and the reaction mechanism. Some new measurements have recently been made[64]. Data below 500 MeV/c would be particularly welcome, since here one enters the region of s–wave dominance of the K^+N amplitude, and a simple picture in terms of a density–dependent effective hard–sphere radius makes sense. The picture above 600 MeV/c is complicated by the formation of possible Z^* resonances[33] in

K^+N partial waves with $l \neq 0$. The $K^+ + {}^4$He system also represents an interesting case for experimental study, since here the central density ρ_0 is higher than that of ordinary nuclear matter, and hence the nucleon "swelling" effects may be amplified.

In summary, the apparent "swelling" of the nucleon needed to explain K^+–nucleus scattering can be understood in terms of a density dependence of the vector–meson masses $m_V(\rho)$ which enter into the K^+N interaction. The density dependence has been estimated by relating $m_V(\rho)$ to the effective nucleon mass $m_N(\rho)$. The discrepancy between first–order "$t\rho$" calculations and the observed $K^+ + {}^{12}$C elastic angular distribution and total cross section is naturally explained in terms of an increased K^+N effective range arising from the decrease of the vector–meson mass in the nucleus.

6. FUTURE PROSPECTS

The next qualitative strides in hypernuclear physics require much higher intensity kaon beams both at low momentum (500 – 800 MeV/c) and above 1.5 GeV/c (for S = −2 studies). Such beams could be provided by a new "kaon factory," although for many experiments, the intensity requirements could be satisfied by upgrading an existing facility such as the Brookhaven AGS (construction of a "booster" is under way at the AGS, and the addition of a stretcher ring would further increase the current to within an order of magnitude of that claimed in kaon factory proposals).

Intense kaon beams would open the door for high resolution studies of hypernuclear structure (presently, we are working with an energy resolution of 3 MeV or so, reminiscent of the status of non–strange nuclear physics several decades ago). One could explore a whole new range of structure questions for heavier hypernuclei with better resolution (rotational and vibrational bands and their coupling, dynamical symmetries (á la the interacting boson model (IBM), for instance) in the presence of the Λ, giant resonances coupled to the Λ, *etc.*). With higher intensity, one could probe, with much greater accuracy, the competition between various weak decay modes of the hypernucleus (pionic versus non–mesonic in light systems, fission versus non–mesonic in heavy systems). The hypernuclear environment affords a unique opportunity to study the four–fermion weak decay ΛN → NN. This process is the ΔS = 1 analog of the parity–violating weak process NN → NN, and is of considerable theoretical interest.

There are also very promising prospects for hypernuclear studies at CEBAF, employing the (γ, K^+) or $(e, e' K^+)$ reactions. Here one would exploit the spin-flip capability of the photon, as opposed to the non-spin-flip (K^-, π^-) or (π^+, K^+) reactions, to populate unnatural parity hypernuclear states. Assuming the existence of a high resolution spectrometer ($\Delta E \approx 100 - 200$ keV) for the K^+, one could hope to measure spin splittings for ground state doublets, at least in favorable cases where the splittings exceed 100 keV and the production cross sections for the natural and unnatural parity members of the doublet are comparable. Studies of hypernuclear γ- rays may also be possible, using a large acceptance detector; weak decays might also be explored.

REFERENCES

1. Gal, A. in Advances in Nuclear Physics, eds. M. Baranger and E. Vogt, Plenum Press, New York (1975), Vol. 8, p. 1.
2. Povh, B., in Annual Review of Nuclear and Particle Science, eds. J. D. Jackson, H. E. Gove and R. F. Schwitters, Annual Reviews, Inc., Palo Alto (1978), Vol. 28, p. 1.
3. Dalitz, R. H., in Proceedings of the International Conference on Nuclear Physics, Berkeley, eds. R. M. Diamond and J. O. Rasmussen, North Holland, Amsterdam (1981), p. 101.
4. Dover, C. B., Nucl. Phys. A374, 359c (1982); in Proceedings of the International Nuclear Physics Conference, Harrogate, England, eds. J. L. Durell, J. M. Irvine and G. C. Morrison, IOP Publishing Ltd, Bristol, Inst. Phys. Conf. Series No. 86 (1987), p. 99; in Proceedings of the International Symposium on Medium Energy Physics, Beijing, eds. Chian Huan-Ching and Zheng Lin-Sheng, World Scientific Publ. Co., Singapore (1987), p. 257.
5. May, M. *et al*, Phys. Rev. Lett. 51, 2085 (1983) and Nucl. Phys. A450, 179c (1986).
6. Millener, D. J., Gal, A., Dover, C. B. and Dalitz, R. H., Phys. Rev. C31, 499 (1985).
7. Bertini, R. *et al*, Phys. Lett. 90B, 375 (1980) and Phys. Lett. 158B, 19 (1985).
8. Piekarz, H. *et al*, Phys. Lett. 110B, 428 (1982).
9. Yamazaki, T. *et al*, Phys. Rev. Lett. 54, 102 (1985).
10. Dover, C. B., Gal, A., Millener, D. J., Physics Reports, to appear; see also Hungerford, E. V., Nucl. Phys. A450, 157c (1986) and Yamazaki, T., Nucl. Phys. A450, 1c (1986).
11. Grace, R. *et al*, Phys. Rev. Lett. 55, 1055 (1985).
12. Dover, C. B., in Few-Body Systems, eds. J. L. Ballot and M. Fabre de la Ripelle, Springer Verlag, Vienna (1987), Suppl. 2, p. 77.
13. Proceedings of the International Symposium on Hypernuclear and Kaon Physics, Brookhaven, ed. R. E. Chrien, Nucl. Phys. A450, 1c-586c (1986).

14. Proceedings of the INS International Symposium on Hypernuclear Physics, Tokyo, eds. H. Bandō, O. Hashimoto and K. Ogawa, Institute for Nuclear Study, University of Tokyo (1986), pp. 1–448.
15. Proceedings of the International Symposium on Strangeness in Hadronic Matter, Bad Honnef, FRG, ed. J. Speth, Nucl. Phys. A479, 1c–466c.
16. Tamura, H. *et al*, Institute for Nuclear Study (Tokyo) preprints INS–Rep.–685 and 686 (June, 1988); Tamura, H. *et al*, Nucl. Phys. A479, 161c (1988).
17. Braun, O. *et al*, Nucl. Phys. B124, 45 (1977); Pigot, C. *et al*, Nucl. Phys. B249, 172 (1985).
18. Piekarz, H., Nucl. Phys. A479, 263c (1988); Tarem, S., PhD Dissertation, Brandeis University, October 1987.
19. Dalitz, R. H. and Deloff, A., Czech. J. Phys. B32, 1021 (1982) and Aust. J. Phys. 36, 617 (1983).
20. Aerts, A. T. M. and Dover, C. B., Phys. Lett. 146B, 95 (1984) and Nucl. Phys. B253, 116 (1985).
21. Piekarz, H. *et al*, AGS experiment 820 (approved).
22. Mulders, P., Aerts, A. T. M, and de Swart, J. J., Phys. Rev. D21, 2653 (1980).
23. Frascaria, R. *et al*, Few–Body Systems, Suppl. 2, 425 (1987).
24. Aerts, A. T. M. and Dover, C. B., Phys. Rev. Lett. 49, 1752 (1982); Phys. Rev. D28, 450 (1983) and D29, 433 (1984).
25. Jaffe, R. L., Phys. Rev. Lett. 38, 195 and 1617(E) (1977).
26. Franklin, G. *et al*, AGS experiment 813 (approved).
27. Franklin, G. *et al*, AGS experiment 835 (approved).
28. Dover, C. B. and Gal, A., Ann. Phys. (NY) 146, 309 (1983).
29. Baltz, A. J., Dover, C. B. and Millener, D. J., Phys. Lett. 123B, 9 (1983).
30. Danysz, M. *et al*, Nucl. Phys. 49, 121 (1963); Prowse, D. J., Phys. Rev. Lett. 17, 782 (1966).
31. Nield, K. J. *et al*, Phys. Rev. C13, 1263 (1976); Bandō, H. *et al*, Institute for Nuclear Study (Tokyo) preprint INS–Rep.–682 (May 1988).
32. Bocquet, J. P. *et al*, Phys. Lett. B182, 146 (1986).
33. Dover, C. B. and Walker, G. E., Physics Reports 89, 1 (1982).
34. Dover, C. B., Ludeking, L. and Walker, G. E., Phys. Rev. C22, 2073 (1980).
35. Feshbach, H. and Kerman, A. K., in Preludes in Theoretical Physics, North Holland, Amsterdam (1965), p. 260.
36. Brückner, W. *et al*, Phys. Lett. 62B, 481 (1976) and 79B, 157 (1978).
37. Donnelly, T. W., Bernstein, A. M. and Epstein, G. N., Nucl. Phys. A358, 195 (1981); Cohen, J., Phys. Rev. C32, 543 (1985).
38. May, M. *et al*, Phys. Rev. Lett. 47, 1106 (1981).
39. Auerbach, E. H. *et al*, Ann. Phys. (NY) 148, 381 (1983).
40. Dalitz, R. H. and Gal, A., Ann. Phys. (NY) 116, 167 (1978).
41. Dalitz, R. H. and Gal, A., Ann. Phys. (NY) 131, 314 (1981).

42. Cohen, S. and Kurath, D., Nucl. Phys. 73, 1 (1965) and Nucl. Phys. A101, 1 (1967).
43. Chrien, R., Nucl. Phys. A478, 705c (1988).
44. Juric, M. *et al*, Nucl. Phys. B52, 1 (1973); Cantwell, T. *et al*, Nucl. Phys. A236, 445 (1974).
45. Lemonne, J. *et al*, Phys. Lett. 18, 354 (1965).
46. Bertini, R. *et al*, Phys. Lett. 83B, 306 (1979) and Nucl. Phys. A360, 315 (1981).
47. Millener, D. J., Dover, C. B and Gal, A., Phys. Rev. C (in press).
48. Negele, J. W. and Vautherin, D., Phys. Rev. C5, 1472 (1972).
49. Rayet, M., Ann. Phys. (NY) 102, 226 (1976) and Nucl. Phys. A367, 381 (1981).
50. Vautherin, D. and Brink, D. M., Phys. Rev. C5, 626 (1972).
51. Myers, W. D., Nucl. Phys. A204, 465 (1973);
Batty, C. J, Gal, A. and Toker, G., Nucl. Phys. A402, 349 (1983).
52. Yamamoto, Y. and Bandō, H., Prog. Theor. Phys. Suppl. 81, 9 (1985) and Prog. Theor. Phys. 73, 905 (1985).
53. Bodmer, A. R. and Usmani, Q. N., Nucl. Phys. A477, 621 (1988).
54. Takeuchi, S. and Shimizu, K., Phys. Lett. 179B, 197 (1986).
55. Dover, C. B. and Gal, A., Prog. in Part. and Nucl. Phys. 12, 171 (1984).
56. Yamamoto, Y., Prog. Theor. Phys. 75, 639 (1986).
57. Kohno, M., Prog. Theor. Phys. 78, 123 (1987).
58. Hungerford, E. V. and Biedenharn, L. C., Phys. Lett. 142B, 232 (1984).
59. Nadeau, H., Nowak, M. A., Rho, M. and Vento, V., Phys. Rev. Lett. 57, 2127 (1986).
60. Brown, G. E., Dover, C. B., Siegel, P. B. and Weise, W., Phys. Rev. Lett. 60, 2723 (1988).
61. Marlow, D. *et al*, Phys. Rev. C25, 2619 (1982).
62. Siegel, P. B., Kaufmann, W. B. and Gibbs, W. R., Phys. Rev. C30, 1256 (1984).
63. Bugg, D. V. *et al*, Phys. Rev. 168, 1466 (1968).
64. Piasetsky, E. and Chrien, R. E., private communication.

DISCLAIMER